FullSWOF: A free software package for the simulation of shallow water flows

Olivier Delestre, Frédéric Darboux, Francois James, Carine Lucas, Christian Laguerre, Stephane Cordier

FullSWOF: A free software package for the simulation of shallow water flows

O. Delestre* F. Darboux† F. James‡ C. Lucas‡
C. Laguerre‡ S. Cordier‡

January 16, 2014

Abstract

Numerical simulations of flows are required for numerous applications, and are usually carried out using shallow water equations. We describe the FullSWOF software which is based on up-to-date finite volume methods and well-balanced schemes to solve this kind of equations. It consists of a set of open source C++ codes, freely available to the community, easy to use, and open for further development. Several features make FullSWOF particularly suitable for applications in hydrology: small water heights and wet-dry transitions are robustly handled, rainfall and infiltration are incorporated, and data from grid-based digital topographies can be used directly. A detailed mathematical description is given here, and the capabilities of FullSWOF are illustrated based on analytic solutions and datasets of real cases. The codes, available in 1D and 2D versions, have been validated on a large set of benchmark cases, which are available together with the download information and documentation at `http://www.univ-orleans.fr/mapmo/soft/FullSWOF/`.

Flow modeling is required in a large variety of natural or man-made situations. Originated by Saint-Venant (Barré de Saint-Venant, 1871) in the study of floods and tides, the description of such phenomena by the so-called shallow water equations has now become classical in flood forecasting, pollutant transport, dam break, tsunami, soil erosion by overland flow, etc. Because in general situations no explicit solutions to the shallow water equations are known, efficient and robust numerical simulations are required.

Over the last forty years, numerous codes have been developed, making use of various methods. The MacCormack scheme has been widely used for scientific purposes (e.g., Zhang and Cundy, 1989; Esteves et al., 2000; Fiedler and Ramirez, 2000). Although it is relatively easy to program and computes quickly, it neither guarantees the positivity of water depths at the wet-dry transitions, nor preserves steady states, i.e., it is not well-balanced (Lee and Wright,

*Corresponding author. Laboratoire J.A. Dieudonné, UMR CNRS 7351, Université de Nice Sophia-Antipolis, Parc Valrose, 06108 NICE Cedex 02, France. Olivier.Delestre@unice.fr.

†Inra, UR0272, UR Science du sol, Centre de recherche Val de Loire, CS 40001, F-45075 Orléans Cedex 2, France.

‡MAPMO, UMR CNRS 7349, Fédération Denis Poisson, FR CNRS 2964, Université d'Orléans, F-45067 Orléans cedex 02, France.

2010), requiring some specific work if these issues shall be addressed (e.g., Esteves et al., 2000; Fiedler and Ramirez, 2000). In the industrial codes used in engineering (e.g., CANOE (Tanguy and Chocat, 2013), HEC-RAS (Brunner, 2010), ISIS (Halcrow, 2012), MIKE11 (DHI Software, 2009)), the flow equations, namely the shallow water equations, are often solved in non-conservative form (Novak et al., 2010) with either Preissmann scheme or Abbott-Ionescu scheme, leading to inaccurate calculations for transcritical flows and hydraulic jumps.

While all these pieces of software have been used for scientific research, the codes of most of them have not been made available to the community, raising a major issue about research reproducibility. Reproducibility is a key component of the scientific method and has received an increasing interest in the recent years in the computer modeling community. In fact numerical simulations rarely ensure this essential property, leading to a low confidence into scientific results and undermining the advance of knowledge (Claerbout and Karrenbach, 1992; Stodden et al., 2013). While the free availability of a source code is not a sufficient condition to make numerical results reproducible, it is a clear necessity (Peng, 2011).

Some programs have adopted a strategy consisting in proposing a set of free, open source codes to solve the shallow water equations (e.g., GeoClaw (Berger et al., 2011), Gerris (Popinet, 2011)). In an explicit effort to facilitate reproducibility in water flow modeling and simulations, and considering that "they are no valuable excuses not to make the code available" (Barnes, 2010), the present paper describes a free software package for the resolution of the shallow water equations: FullSWOF. The source code of FullSWOF has been made public under a license that grants the freedoms to use, study, share, and modify it. The use of a standard version of C++ (ANSI) helps in easing accessibility to numerous users, both in the education, in the science and in the industry.

FullSWOF has been developed by a joint effort of mathematicians and hydrologists. Using a set of analytic solutions to the shallow water equations detailed in Delestre et al. (2013), FullSWOF includes a validation procedure that guarantees reproducibility to the users and non-regression to the developers. This procedure is, together with the version control system, the bug tracking, etc., part of the quality assurance of FullSWOF. These also facilitate contributions by third parties and make their inclusion clearly identifiable. To make its use and development easier, a graphic user interface and both a one-dimensional and a two-dimensional versions have been released. FullSWOF can also be included in third parties software, as already done by openLISEM from version 1.67 (Baartman et al., 2013).

As the GeoClaw and Gerris programs, FullSWOF makes use of finite volume methods, but specific features make it more oriented towards applications in hydrology, hence its name: FullSWOF stands for *Full S*hallow *W*ater equations for *O*verland *F*low. In this context, it solves the complete shallow water equations and not solely one of their approximations, such as the diffusive wave or the kinematic wave (Moussa and Bocquillon, 2000; Novak et al., 2010). It makes use of the finite volume method, which is preferred to the finite difference method, because it ensures the mass conservation and the positivity of water depth. A well-balanced scheme guaranties the preservation of steady states. Special attention has been paid to specific hydrological features: transitions between wet and dry areas, small water heights, various friction models.

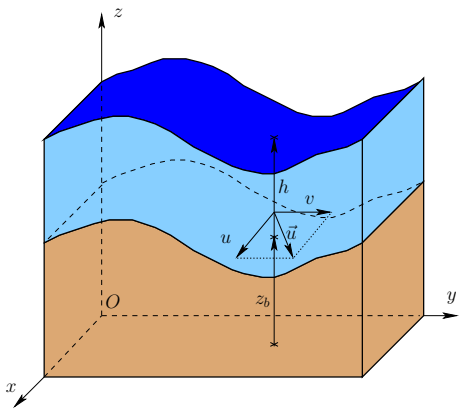

Figure 1: Notations for 2D shallow water equations.

The software program incorporates rainfall and infiltration, and makes possible the direct use of digital topographic grids.

After presenting the physically-based model (section 1) and its most important properties (section 2), the numerical methods are described in section 3. Then we proceed with the description of the FullSWOF program in section 4. Finally, in section 5, comparisons are made with explicit solutions representative of a wide variety of flow conditions, and application to three real cases — a laboratory experiment, rain on a field plot, and a dam break — are reported.

1 Model: Shallow Water Equations

1.1 General Settings

The system of shallow water equations is a simplified model for a class of free boundary incompressible Navier-Stokes flows that can occur in rivers or channels, in the ocean (tides, tsunami), but also in agricultural overland flow. They are characterized by the fact that the water height $h(t,x,y)$ [L] is small with respect to the horizontal dimensions of the considered domain (Figure 1 and Hervouet (2007, chap. 2)). In this context, two main hypotheses are assumed. First, the fluid velocity is constant along the vertical direction, so that we can use the horizontal components of the vertically-averaged velocity $u(t,x,y)$ and $v(t,x,y)$ [L/T] instead of the three-component Navier-Stokes velocity vector. Next, the pressure in the fluid is hydrostatic, so that after integration along the vertical direction z the pressure field is given by $p(t,x,y) = gh(t,x,y)^2/2$, where g is the gravity constant [L/T^2].

Under these assumptions, the averaged Navier-Stokes system can be rewrit-

ten as the following balance laws

$$\left\{\begin{array}{rcl} \partial_t h + \partial_x (hu) + \partial_y (hv) & = & R - I, \\ \partial_t (hu) + \partial_x \left(hu^2 + \dfrac{gh^2}{2} \right) + \partial_y (huv) & = & gh(S_{0x} - S_{fx}), \\ \partial_t (hv) + \partial_x (huv) + \partial_y \left(hv^2 + \dfrac{gh^2}{2} \right) & = & gh(S_{0y} - S_{fy}). \end{array}\right. \tag{1}$$

The first equation is actually the exact integrated form of the incompressibility condition, and hence it is a mass balance. The other two equations are momentum balances and involve forces such as gravity and friction. In particular, the $gh^2/2$ term is the hydrostatic pressure. Let us now describe each term, recalling their physical dimensions:

1. z_b is the topography [L]. Since we consider no erosion here, it is a given function of space, $z_b(x, y)$, and we classically denote by S_{0x} and S_{0y} the opposites of the slopes in the x and y directions respectively, $S_{0x} = -\partial_x z_b(x, y)$ and $S_{0y} = -\partial_y z_b(x, y)$.
2. R is the rain intensity [L/T]. It is a given function $R(t, x, y) \geq 0$. In the current versions of FullSWOF, we consider the rain to be uniform in space.
3. I is the infiltration rate [L/T]. This term $I(t, x, y) \geq 0$ is defined through the coupling with an infiltration model such as the bi-layer Green-Ampt model (section 1.3).
4. $S_f = \left(S_{fx}, S_{fy}\right)$ is the friction force, which is in general a nonlinear function of the velocity and the water height (section 1.2).

We shall pay a particular attention to the one-dimensional version of system (1) because, on the one hand, it has practical applications when the flow can be considered homogeneous or when the effect of the edges can be neglected (e.g., wide channels, flood propagation in river networks), and, on the other hand, its study gives a better insight of the complete two-dimensional model, from both theoretical and numerical viewpoints. It writes

$$\left\{\begin{array}{rcl} \partial_t h + \partial_x (hu) & = & R - I, \\ \partial_t (hu) + \partial_x \left(hu^2 + \dfrac{gh^2}{2} \right) & = & gh(S_{0x} - S_{fx}). \end{array}\right. \tag{2}$$

In both systems (1) and (2), the homogeneous part, that is the left-hand side, is called the transport (or convection) operator. It corresponds to the flow of an ideal fluid on a flat bottom, without friction, rain or infiltration. In the one-dimensional setting, this is exactly the model introduced by Barré de Saint-Venant (1871). This operator contains several important properties of the flow, hence in sections 2 and 3 we perform a careful analysis of the homogeneous system, considering both theoretical and numerical studies.

1.2 Friction Terms

Friction terms depend on the flow velocity. In the formulæ below, $\vec{u}$ is the velocity vector $\vec{u} = (u, v)$ with $|\vec{u}| = \sqrt{u^2 + v^2}$ and $\vec{q}$ is the discharge $\vec{q} =$

$(hu, hv) = h\vec{u}$. In hydrological models, there are two families of friction laws, based on empirical considerations. On the one hand, the Manning-Strickler friction law reads

$$S_f = C_f \frac{\vec{u}|\vec{u}|}{h^{4/3}} = C_f \frac{\vec{q}|\vec{q}|}{h^{10/3}}, \tag{3}$$

with $C_f = n^2$ or $C_f = 1/K^2$, where n is the Manning coefficient [$L^{-1/3}T$] and K is the Strickler coefficient [$L^{-1/3}T^{-1}$] respectively (Chow, 1959). On the other hand, the laws of Darcy-Weisbach and Chézy write

$$S_f = C_f \frac{\vec{u}|\vec{u}|}{h} = C_f \frac{\vec{q}|\vec{q}|}{h^3}. \tag{4}$$

Taking $C_f = f/(8g)$, with f a dimensionless coefficient, or $C_f = 1/C^2$, C [$L^{1/2}T^{-1}$] we get the Darcy-Weisbach or Chézy friction law respectively. Readers are referred to the chapter 5 of Chow (1959) for details and examples about friction laws. Notice that the friction force may depend on the space variable, especially on large domains, but this is not considered in the following.

1.3 Infiltration Model

Infiltration is computed at each cell using a Green-Ampt model (Green and Ampt, 1911; Mein and Larson, 1973). The main idea is to assume the water infiltrates as an advancing wetting front (at the depth $Z_f = Z_f(t)$), from a fully saturated zone (with moisture content θ_s) to another zone with the initial water content θ_i (Figure 2a).

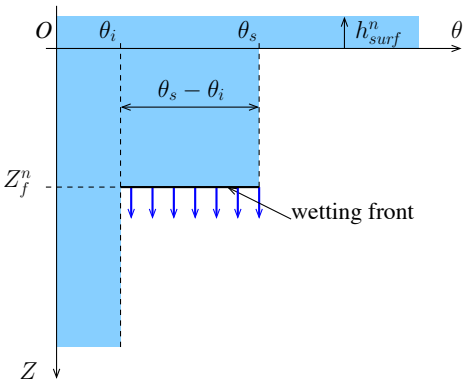

(a) Wetting front.

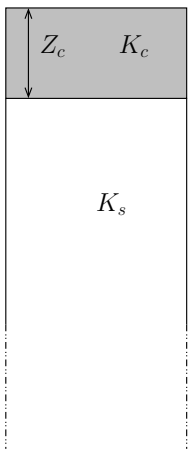

(b) Geometry of the bi-layer model.

Figure 2: Notations for the Green-Ampt infiltration model.

Following Esteves et al. (2000), we implemented a bi-layer Green-Ampt model (Hillel and Gardner, 1970; Delestre, 2010) in which the upper layer is characterized by its thickness Z_c and its hydraulic conductivity K_c, and the second layer has an infinite extension and a hydraulic conductivity K_s (Figure 2b).

Note that the 'c' and 's' subscripts stand for 'crust' and 'soil' respectively. Z_c can be set equal to zero for cases where a single layer model is relevant. In the following, we assume that the infiltration parameters can vary in space, but are uniform in time.

At each cell, when there is water at the surface, the infiltration capacity I_C [L/T] at time t_n is given by:

$$I_C(t_n) = I_C^n = \begin{cases} K_s \left(1 + \dfrac{h_f - h_{surf}^n}{Z_f^n}\right) & \text{if} \quad Z_c = 0, \\ K_c \left(1 + \dfrac{h_f - h_{surf}^n}{Z_f^n}\right) & \text{if} \quad Z_f^n \leq Z_c, \\ K_e^n \left(1 + \dfrac{h_f - h_{surf}^n}{Z_f^n}\right) & \text{else.} \end{cases} \tag{5}$$

In these equalities, $K_e^n = K_e(t_n)$ is the effective hydraulic conductivity at time t_n:

$$K_e^n = \frac{Z_f^n}{\dfrac{Z_f^n - Z_c}{K_s} + \dfrac{Z_c}{K_c}} = \frac{1}{\dfrac{1}{K_s}\left(1 - Z_c \dfrac{\Delta\theta}{V_{inf}^n}\right) + Z_c \dfrac{\Delta\theta}{V_{inf}^n}\dfrac{1}{K_c}}.$$

The value of h_f depends on the soil; it is sometimes denoted by Ψ in the literature and represents the suction head at the wetting front. The (positive) quantity $-h_{surf}^n = -h_{surf}(t_n)$ is the water height at the surface of the cell that is available for infiltration at the time t_n. Finally, $Z_f^n = Z_f(t_n)$ is the gravity force over the water column at time t_n and can be written as $Z_f^n = V_{inf}^n/\Delta\theta$, where V_{inf}^n is the infiltrated volume at time t_n and $\Delta\theta = \theta_s - \theta_i$.

To avoid an infinite infiltration rate at the beginning (when the infiltrated volume is still equal to zero), we add a threshold to get the infiltration rate $I^n = \min(I_C^n, i_{max})$. Because the infiltrated volume cannot exceed the water height at the surface, it is updated as follows:

$$V_{inf}^{n+1} = V_{inf}^n + \min(-h_{surf}^n, I^n \times \Delta t)$$

Finally, the water height at the surface is updated.

2 Properties

In this section, we recall several mathematical properties of the shallow water model, for both the 1D and 2D cases.

2.1 One-Dimensional Model

In order to emphasize the mathematical properties of the shallow water model, we first rewrite the one-dimensional homogeneous equations using vectors:

$$\partial_t W + \partial_x F(W) = 0, \quad \text{where } W = \begin{pmatrix} h \\ hu \end{pmatrix}, \quad F(W) = \begin{pmatrix} hu \\ hu^2 + \dfrac{gh^2}{2} \end{pmatrix}, \tag{6}$$

with $F(W)$ the flux of the equation. The transport is more clearly evidenced in the following non-conservative form:

$$\partial_t W + A(W)\partial_x W = 0, \quad A(W) = F'(W) = \begin{pmatrix} 0 & 1 \\ -u^2 + gh & 2u \end{pmatrix},$$

where $A(W)$ is the matrix of transport coefficients. More precisely, when $h > 0$, the matrix $A(W)$ turns out to be diagonalizable, with eigenvalues $\lambda_1(W) = u - \sqrt{gh} < u + \sqrt{gh} = \lambda_2(W)$. This important property of having two real and distinct eigenvalues is called strict hyperbolicity (e.g., Godlewski and Raviart (1996) and references therein for more details). The eigenvalues are the velocities of surface waves of the fluid, which are the fundamental characteristics of the flow. Notice here that the eigenvalues coincide if $h = 0$, that is for dry zones. In that case, the system is no longer hyperbolic, which induces difficulties at both theoretical and numerical levels.

From these formulæ we recover a useful classification of flows, based on the relative values of the velocities of the fluid, u, and of the waves, $\sqrt{gh}$. Indeed if $|u| < \sqrt{gh}$ the characteristic velocities $u - \sqrt{gh}$ and $u + \sqrt{gh}$ have opposite signs, and information propagate upward as well as downward: the flow is said to be subcritical or fluvial. On the other hand, when $|u| > \sqrt{gh}$, all the information is going downward, and the flow is said to be supercritical or torrential.

This classification has consequences for the numerical scheme. Since we have two unknowns h and u (or equivalently h and $q = hu$), a subcritical flow is determined by one upstream value and one downstream value, whereas a supercritical flow is completely determined by the two upstream values. Thus for numerical simulations, we use only one of the two variables for a subcritical inflow/outflow boundary. For a supercritical inflow boundary, we have to impose both variables, and, for a supercritical outflow boundary, the Neumann free boundary conditions are considered (e.g., Bristeau and Coussin, 2001). In this context, it is useful to be able to determine whether the flow is subcritical or supercritical. To this end, we can consider two quantities. The first one is the Froude number, given by

$$\mathrm{Fr} = \frac{|u|}{\sqrt{gh}}.$$

The flow is subcritical or supercritical if $\mathrm{Fr} < 1$ or $\mathrm{Fr} > 1$, respectively. A more visual criterion is obtained through the so-called critical height h_c which writes

$$h_c = \left(\frac{|q|}{\sqrt{g}}\right)^{2/3},$$

for a given discharge $q = hu$. The flow is subcritical or supercritical if $h > h_c$ or $h < h_c$, respectively.

2.2 Source Terms and Equilibria

When source terms (e.g., topography, rain or friction) are involved, other properties have to be considered, in particular the occurrence of steady-state (or

equilibrium) solutions, that is solutions which do not depend on time ($\partial_t \equiv 0$). This amounts to some balance between the flux and the source terms:

$$\partial_x(hu) = R - I, \quad \partial_x\left(hu^2 + \frac{gh^2}{2}\right) = gh(S_{0x} - S_{fx}).$$

Among these solutions, the homogeneous states are of particular interest, namely the so-called parallel flows

$$\partial_x(hu) = R - I = 0, \quad gh(S_{0x} - S_{fx}) = 0,$$

and lakes or puddles at rest

$$u = 0, \quad h + z = \text{const.}$$

These solutions are important for two reasons: on the one hand, specific numerical methods have to be designed in order to be able to capture them; on the other hand, they furnish several explicit solutions that can be used as test cases for numerical methods (see section 5 and Delestre et al. (2013)).

2.3 Two-Dimensional Model

The two-dimensional shallow water system (1) can be written under the following conservative form:

$$\partial_t U + \partial_x G(U) + \partial_y H(U) = S(U, t, x, y), \tag{7}$$

where

$$U = \begin{pmatrix} h \\ hu \\ hv \end{pmatrix}, \quad G(U) = \begin{pmatrix} hu \\ hu^2 + \dfrac{gh^2}{2} \\ huv \end{pmatrix}, \quad H(U) = \begin{pmatrix} hv \\ huv \\ hv^2 + \dfrac{gh^2}{2} \end{pmatrix}$$

and

$$S(U, t, x, y) = \begin{pmatrix} R - I \\ gh(S_{0x} - S_{fx}) \\ gh(S_{0y} - S_{fy}) \end{pmatrix}.$$

If we denote by DG_x and DH_y the Jacobian matrices of the fluxes, namely

$$DG_x = \begin{pmatrix} 0 & 1 & 0 \\ -u^2 + gh & 2u & 0 \\ -uv & v & u \end{pmatrix} \quad \text{and} \quad DH_y = \begin{pmatrix} 0 & 0 & 1 \\ -uv & v & u \\ -v^2 + gh & 0 & 2v \end{pmatrix},$$

system (7) reads

$$\partial_t U + DG_x\, \partial_x U + DH_y\, \partial_y U = S(U, t, x, y).$$

The notion of hyperbolicity is defined here, following Godlewski and Raviart (1996), by studying the flow along any direction. For any unit vector $\xi = (\xi_x, \xi_y) \in \mathbb{R}^2$, the velocity of the flow in the ξ direction is by definition $u_\xi =$

$\xi_x u + \xi_y v$, and we define some kind of directional derivative as: $DF(\xi) = \xi_x DG_x + \xi_y DH_y$. Then one can check that $DF(\xi)$ has three eigenvalues:

$$\lambda_1(\xi) = u_\xi - \sqrt{gh}, \quad \lambda_2(\xi) = u_\xi \quad \text{and} \quad \lambda_3(\xi) = u_\xi + \sqrt{gh}. \tag{8}$$

Outside the dry zones, that is if $h > 0$, the three eigenvalues satisfy $\lambda_1(\xi) < \lambda_2(\xi) < \lambda_3(\xi)$, therefore the matrix $DF(\xi)$ is diagonalizable for all ξ: the system (7) is strictly hyperbolic. As in the one-dimensional case, this property is no longer true inside the dry zones.

3 Numerical Methods

In this section, we detail the numerical methods well-adapted to the resolution of the shallow water system and implemented in FullSWOF. For the resolution, the shallow water system is divided in two parts: the transport (i.e., convective) operator and the source terms. First, we perform a convective step, where the homogeneous part of the system is solved by a finite volume strategy. This leads to a first-order accurate scheme, the second order accuracy in space being obtained by reconstruction techniques. Second, this scheme is coupled with the source terms, and specific methods are used to take into account steady states. In case a second order approximation in time is looked for, Heun's method is used. These steps are described below in detail for the one-dimensional setting, then extended to the two-dimensional case.

3.1 General Settings

Let us first introduce several notations which will be used throughout this section. First consider the time discretization: let $t^0 = 0$ be the initial time, we fix a time step $\Delta t > 0$, and for $n \geq 0$ we set $t^{n+1} = t^n + \Delta t$. Next, the space discretization is defined by constant positive space steps, Δx in one dimension, $(\Delta x, \Delta y)$ in two space dimensions, where a rectangular mesh is assumed. Finally, we compute piecewise constant approximations of the vectors W (in 1D) or U (in 2D). More precisely, W_i^n and U_{ij}^n are constant approximations of W on $[t^n, t^{n+1}[\times]x_{i-1/2}, x_{i+1/2}[$ and of U on $[t^n, t^{n+1}[\times]x_{i-1/2}, x_{i+1/2}[\times]y_{j-1/2}, y_{j+1/2}[$, respectively (see Figure 3 for details of notations).

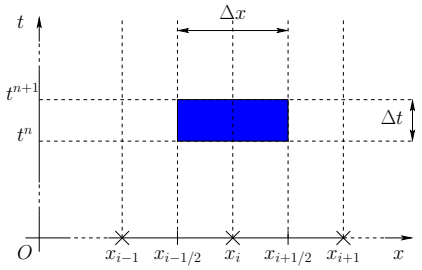

(a) One-dimensional time and space discretization.

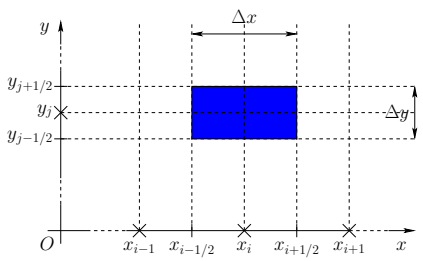

(b) Two-dimensional space discretization for every time step.

Figure 3: Discretization of time and space in FullSWOF.

For each $n \geq 1$, we compute the components of W^n and U^n by explicit schemes in time which take the general recursive form

$$W_i^{n+1} = W_i^n - \Delta t \Phi(W^n), \quad U_{ij}^{n+1} = U_{ij}^n - \Delta t \Phi(U^n). \tag{9}$$

At this point, we briefly recall several fundamental properties required for an effective numerical scheme (for detailed definitions, see Godlewski and Raviart (1996)). First, the consistency error quantifies the ability of the scheme to mimic the equation. It is obtained by replacing each occurrence of W_i^n in the formula (9) by the exact solution $W(t^n, x_i)$. If this error goes to 0 when Δt and $\Delta x \to 0$, the scheme is consistent. If the error behaves as $O(\Delta t^q + \Delta x^p)$, the scheme is of order q in time and p in space. Next, one is concerned with stability, a notion that can take various forms. Usually, it is formulated by stating that a given norm of the numerical solution at time t^n is controlled by the norm at time 0. Regarding the shallow water equations, a particularly important stability property is the preservation of the positivity of the water height, especially if wet-dry transitions and thin water layers are to be simulated. Formula (9) is nothing more than an Euler scheme in time, where the function Φ is some discretization of the space derivatives and of the source terms. Formula (9) defines a first-order scheme in time, regardless of the definition of Φ. There are several ways to increase the accuracy of such schemes, following standard methods to solve ordinary differential equations. We choose here Heun's method (also referred as the modified Euler method), which is a prediction-correction method. In the first two formulæ below, W_i^* and W_i^{**} are the predicted values, the last one is the correction step:

$$W_i^* = W_i^n - \Delta t \Phi(W^n), \quad W_i^{**} = W_i^* - \Delta t \Phi(W^*), \qquad W_i^{n+1} = \frac{W_i^n + W_i^{**}}{2}.$$

When Φ is determined, the numerical scheme is complete. The remaining of this section explains step by step how to build the function Φ, which encodes all the stability and accuracy properties of the scheme in the space variables.

3.2 Convective Step for the One-Dimensional Model

In order to solve system (2), the first step consists in using a finite volume strategy to solve the homogeneous system (6). The idea is to integrate the system of equations on each time-space cell as depicted by the blue rectangle in Figure 3a. We obtain the following approximation formula

$$W_i^{n+1} = W_i^n - \frac{\Delta t}{\Delta x}(F_{i+1/2}^n - F_{i-1/2}^n), \tag{10}$$

where $F_{i+1/2}^n$ and $F_{i-1/2}^n$ are approximations of the flux on the edges $x_{i+1/2}$ and $x_{i-1/2}$, respectively. At this stage, the finite volume scheme is not completely determined yet: we need to specify a formula to compute this flux approximation on each edge. We choose here to set, for all indexes i, $F_{i+1/2}^n = \mathcal{F}(W_i^n, W_{i+1}^n)$, where $\mathcal{F}(W_L, W_R)$ is called the numerical flux, a given function of the states on the left and right of the interface.

Among the numerical fluxes proposed in the literature, such as Rusanov, HLL, VFRoe-ncv, kinetic (see Bouchut (2004) for explicit formulæ and additional references), several are available in FullSWOF. In this paper, we choose

to present the HLL flux (introduced in Harten et al. (1983)) because it offers a good compromise between simplicity, computing time and robustness as shown numerically in Delestre (2010). It writes

$$\mathcal{F}(W_L, W_R) = \begin{cases} F(W_L) & \text{if } 0 \leq c_1 \\ \dfrac{c_2 F(W_L) - c_1 F(W_R)}{c_2 - c_1} + \dfrac{c_1 c_2}{c_2 - c_1}(W_R - W_L) & \text{if } c_1 < 0 < c_2 \\ F(W_R) & \text{if } c_2 \leq 0 \end{cases}, \tag{11}$$

with two parameters $c_1 < c_2$ which are the approximations of the slowest and fastest wave speeds, respectively. We refer to Batten et al. (1997) for further discussion on the wave speed estimates. In FullSWOF, we have implemented

$$c_1 = \inf_{W=W_L,W_R} \left(\inf_{j\in\{1,2\}} \lambda_j(W) \right) \text{ and } c_2 = \sup_{W=W_L,W_R} \left(\sup_{j\in\{1,2\}} \lambda_j(W) \right),$$

where $\lambda_1(W) = u - \sqrt{gh}$ and $\lambda_2(W) = u + \sqrt{gh}$ are the eigenvalues of the one-dimensional model (section 2.1). This numerical flux is said to be upwind, i.e., it mimics the waves propagation. Indeed when the flow is supercritical ($0 \leq c_1$ or $c_2 \leq 0$), all information are going from upstream to downstream, thus the numerical flux is calculated from upstream values only. While for subcritical flow ($c_1 < 0 < c_2$), information are coming from both upstream and downstream, thus the flux is calculated using both upstream and downstream values.

As described above, except for a few specific numerical fluxes, the scheme is first-order accurate in space. To obtain second order accuracy, we perform a linear reconstruction on the variables $W = (h, hu)$, thus obtaining new variables on each interface $i + 1/2$, namely $W_{i+1/2-}$ on the left, $W_{i+1/2+}$ on the right. Using $\mathcal{F}(W_{i+1/2-}, W_{i+1/2+})$ in the finite volume scheme instead of $\mathcal{F}(W_i^n, W_{i+1}^n)$ leads to a second order approximation in space. Among the existing formulæ for the linear reconstruction (e.g., MUSCL, ENO, see Bouchut (2004)), several are implemented in FullSWOF.

We conclude this section by an important remark about time discretization. Explicit schemes imply a control on the time step, which cannot be too large for a given space step. More precisely, for a three-point scheme as defined above (W_i^{n+1} depends only on W_{i-1}^n, W_i^n and W_{i+1}^n), the numerical speed of propagation is $\Delta x/\Delta t$. To avoid any loss of information, this velocity has to be larger than any possible physical velocity, which reads

$$C\frac{\Delta x}{\Delta t} \geq \sup_{(t,x)} \left\{ |u(t,x)| + \sqrt{gh(t,x)} \right\},$$

where the supremum is taken over the whole time-space domain of interest and C is a parameter depending on the dimension and on the order of the scheme which are considered (in 1D, at the first order $C = 1$ and at the second order $C = 0.5$; in 2D, at the first order $C = 0.5$ and at the second order $C = 0.25$). When this condition is violated, the scheme becomes unstable, and oscillations appear. This theoretical formulation of the limitation, known as the CFL condition (Courant, Friedrichs, Lewy) (Godlewski and Raviart, 1996), is hardly useful because, due to the nonlinearity, the right-hand side is difficult to estimate. On the other hand, even if one gets such an estimate, it can lead to

an underestimated fixed time step when there are no large variations of h and u. Thus the computation of the time step could be replaced by a sequence of variable time steps Δt^n according to the following rule:

$$\Delta t^n = \frac{C\Delta x}{\sup_i\{|u_i^{n-1}| + \sqrt{gh_i^{n-1}}\}}. \tag{12}$$

However, when water heights converge toward zero, time steps will tend to become infinite, which is not reasonable. Consequently, we add an upper bound to the computation, which leads to the following formulation, implemented in FullSWOF_2D:

$$\Delta t^n = C \min\left(\Delta x, \frac{\Delta x}{\sup_i\{|u_i^{n-1}| + \sqrt{gh_i^{n-1}}\}}\right).$$

3.3 Source Terms

When source terms are involved, specific methods have to be introduced to capture equilibrium states. Numerical schemes that preserve stationary equilibria are called equilibrium schemes, or well-balanced schemes (Bermúdez and Vázquez, 1994; Greenberg and LeRoux, 1996). A first class of methods consists in splitting-type methods, where the transport equation and the source term are solved somehow independently. Another strategy consists in applying a specific reconstruction technique, thus modifying the flux computation. It turns out that this last method is well adapted to the topography term, but not quite so for the friction term. Hence, in FullSWOF, these two approaches are used: the topography is solved using a well-balanced scheme (section 3.3.1) and the friction with a semi-implicit method (section 3.3.2).

3.3.1 The Hydrostatic Reconstruction

The hydrostatic reconstruction (Audusse et al., 2004; Bouchut, 2004), as its name suggests, reconstructs new variables to be injected in the numerical flux. It is designed to get a well-balanced scheme, in the sense that it preserves at least the steady state at rest (i.e., the hydrostatic equilibrium), as well as the positivity of the water height. The hydrostatic reconstruction procedure is applied at once to the original variables W_i^n, thus leading to a first-order scheme.

Here, we detail how to get a second order version, which is used in FullSWOF. The second order scheme consists in first performing the linear reconstruction (chosen for the convective step), not only to $W = (h, hu)$ as before, but also to $h + z_b$. Then, the hydrostatic reconstruction is applied to these modified variables. Notice that this strategy introduces an artificial time dependence on the topography, which is in some sense reconstructed as well. This is mandatory to cope with steady equilibrium states and preserve the positivity of h (Audusse et al., 2004). The linear reconstruction gives values $(h_{i+1/2-}, z_{i+1/2-}, u_{i+1/2-})$ on the left of the interface $i + 1/2$, and $(h_{i+1/2+}, z_{i+1/2+}, u_{i+1/2+})$ on its right.

The final formula for the hydrostatic reconstruction can now be written as

$$\begin{cases} h_{i+1/2L} = \max\left(h_{i+1/2-} + z_{i+1/2-} - \max\left(z_{i+1/2-}, z_{i+1/2+}\right), 0\right), \\ W_{i+1/2L} = \begin{pmatrix} h_{i+1/2L} \\ h_{i+1/2L} u_{i+1/2-} \end{pmatrix}, \\ h_{i+1/2R} = \max\left(h_{i+1/2+} + z_{i+1/2+} - \max\left(z_{i+1/2-}, z_{i+1/2+}\right), 0\right), \\ W_{i+1/2R} = \begin{pmatrix} h_{i+1/2R} \\ h_{i+1/2R} u_{i+1/2+} \end{pmatrix}. \end{cases} \tag{13}$$

For a given space discretization, it may exhibit abnormal behaviors for some combinations of slope and water height (Delestre et al., 2012). Particularly obvious for the order one scheme and on a coarse mesh, they disappear when refining the mesh, and are hardly noticeable at order two.

When applying the hydrostatic reconstruction, formula (10) has to be modified to preserve the consistency of the scheme. It rewrites $W_i^{n+1} = W_i^n - \Delta t \Phi(W^n)$ with

$$\Phi(W^n) = \frac{1}{\Delta x}\left(F_{i+1/2L}^n - F_{i-1/2R}^n - Fc_i^n\right),$$

where $F_{i+1/2L}^n$ and $F_{i-1/2R}^n$ are given by

$$\begin{cases} F_{i+1/2L}^n = \mathcal{F}(W_{i+1/2L}^n, W_{i+1/2R}^n) + \begin{pmatrix} 0 \\ \frac{g}{2}\left(\left(h_{i+1/2-}^n\right)^2 - \left(h_{i+1/2L}^n\right)^2\right) \end{pmatrix}, \\ F_{i-1/2R}^n = \mathcal{F}(W_{i-1/2L}^n, W_{i-1/2R}^n) + \begin{pmatrix} 0 \\ \frac{g}{2}\left(\left(h_{i-1/2+}^n\right)^2 - \left(h_{i-1/2R}^n\right)^2\right) \end{pmatrix}, \end{cases}$$

where $W_{i+1/2L}^n$ and $W_{i+1/2R}^n$ are computed by formula (13). The additional centered term Fc_i^n is determined to preserve consistency and well-balancing (Audusse et al., 2004):

$$Fc_i^n = \begin{pmatrix} 0 \\ -\frac{g}{2}\left(h_{i-1/2+}^n + h_{i+1/2-}^n\right)\left(z_{i+1/2-}^n - z_{i-1/2+}^n\right) \end{pmatrix}.$$

3.3.2 Friction

A possible way to handle friction in a well-balanced scheme consists in first introducing the friction in the topography term, and then applying the hydrostatic reconstruction (section 3.3.1): this approach is therefore named "apparent topography". This method has been used for example to solve the shallow water system with a Coriolis force (Bouchut, 2004) and with a Coulomb friction (Bouchut, 2004; Mangeney et al., 2007). The main idea is to use the modified topography z_{app} defined by $z_{app} = z_b - b$, with $\partial_x b = S_{fx}$. The use of this class of methods gives rise to a well-balanced scheme for friction as well as topography, hence computing neatly equilibrium states. However it is not completely satisfactory on transitory solutions, as noticed in Delestre et al. (2009) and Delestre and James (2010): a spurious peak appears at the wet-dry front before the equilibrium is reached. Therefore we turned to splitting methods. The explicit discretization, despite its simplicity, is not relevant for the type of problems

we are interested in because it leads to instabilities and overestimates of the velocity at wet-dry interfaces (Paquier, 1995). On the other hand, the fully implicit method has a high computational cost, and cannot be generalized to the two-dimensional system due to the nonlinear form of the friction law. Another possibility consists in using a Strang time splitting to reach the second order in time, however this leads to a more complicated algorithm and, moreover, there is no significant gain in accuracy compared to first-order methods (Liang and Marche, 2009). Finally, it turns out that the best compromise between accuracy, stability and computational complexity lies in semi-implicit methods (Fiedler and Ramirez, 2000; Bristeau and Coussin, 2001; Liang and Marche, 2009). We choose the semi-implicit treatment proposed in Bristeau and Coussin (2001), not only because it preserves steady states at rest, but also for its stability. At the first order in time, after a convective step $W_i^* = W_i^n - \Delta t \Phi(W^n)$, the value W_i^{n+1} is given by:

$$W_i^{n+1} = \begin{pmatrix} h_i^{n+1} \\ q_i^{n+1} \end{pmatrix} = \begin{pmatrix} h_i^* \\ q_i^* \left(1 + g n^2 \Delta t \dfrac{|q_i^n|}{h_i^n \left(h_i^{n+1} \right)^{4/3}} \right)^{-1} \end{pmatrix}$$

for the Manning friction law (3), and by

$$W_i^{n+1} = \begin{pmatrix} h_i^{n+1} \\ q_i^{n+1} \end{pmatrix} = \begin{pmatrix} h_i^* \\ q_i^* \left(1 + \Delta t \dfrac{f}{8} \dfrac{|q_i^n|}{h_i^n h_i^{n+1}} \right)^{-1} \end{pmatrix}$$

for the Darcy-Weisbach friction law (4). Notice the simplicity of the method, which gives an explicit value for W_i^{n+1}.

3.3.3 Rain and Infiltration

Unlike the friction and the topography source terms, rain and infiltration involve no particular numerical difficulties such as steady-state or stability preservations. Moreover, dealing with infiltration implicitly would make more difficult the integration of other infiltration models (such as Richard's or Darcy's models) into FullSWOF. For these reasons, we have chosen to treat the rain and infiltration terms explicitly.

3.4 Convective Step for the Two-Dimensional Model

In general, the 2D system can be treated in the same way as the 1D system because calculations are done on each interface of each cell (and so do not depend on the cell geometry). Digital elevation models (DEM) (i.e., digital topographic maps) are mainly represented as structured grids. Some DEM can be represented as a vector-based triangular network (TIN). Because TIN can easily be converted into DEM, we chose to make developments dedicated to structured meshes (Figure 3b). To get a 2D version, we perform the linear reconstruction of U and z_b and the hydrostatic reconstruction as in one dimension (equation (13)). We get $U_{\bullet_L,\bullet}$ and $U_{\bullet_R,\bullet}$ along the x-direction, and $U_{\bullet,\bullet_L}$ and $U_{\bullet,\bullet_R}$ along the y-direction.

Then, the two-dimensional finite volume scheme reads

$$U^*_{i,j} = U^n_{i,j} - \frac{\Delta t}{\Delta x}\left(G^n_{i+1/2L,j} - G^n_{i-1/2R,j} - Gc^n_{i,j}\right) - \frac{\Delta t}{\Delta y}\left(H^n_{i,j+1/2L} - H^n_{i,j-1/2R} - Hc^n_{i,j}\right)$$

with

$$\begin{cases} G^n_{i+1/2L,j} = \mathcal{G}\left(U^n_{i+1/2L,j}, U^n_{i+1/2R,j}\right) + S^n_{i+1/2L,j}, \\ G^n_{i-1/2R,j} = \mathcal{G}\left(U^n_{i-1/2L,j}, U^n_{i-1/2R,j}\right) + S^n_{i-1/2R,j}, \\ H^n_{i,j+1/2L} = \mathcal{H}\left(U^n_{i,j+1/2L}, U^n_{i,j+1/2R}\right) + S^n_{i,j+1/2L}, \\ H^n_{i,j-1/2R} = \mathcal{H}\left(U^n_{i,j-1/2L}, U^n_{i,j-1/2R}\right) + S^n_{i,j-1/2R}, \end{cases}$$

where

$$S^n_{i+1/2L,j} = \begin{pmatrix} 0 \\ \frac{g}{2}\left(\left(h^n_{i+1/2-,j}\right)^2 - \left(h^n_{i+1/2L,j}\right)^2\right) \\ 0 \end{pmatrix},$$

$$S^n_{i-1/2R,j} = \begin{pmatrix} 0 \\ \frac{g}{2}\left(\left(h^n_{i-1/2+,j}\right)^2 - \left(h^n_{i-1/2R,j}\right)^2\right) \\ 0 \end{pmatrix},$$

$$S^n_{i,j+1/2L} = \begin{pmatrix} 0 \\ 0 \\ \frac{g}{2}\left(\left(h^n_{i,j+1/2-}\right)^2 - \left(h^n_{i,j+1/2L}\right)^2\right) \end{pmatrix},$$

$$S^n_{i,j-1/2R} = \begin{pmatrix} 0 \\ 0 \\ \frac{g}{2}\left(\left(h^n_{i,j-1/2+}\right)^2 - \left(h^n_{i,j-1/2R}\right)^2\right) \end{pmatrix}.$$

$\mathcal{G}$ and $\mathcal{H}$ are the numerical fluxes for the resolution of the homogeneous system. The first two components of $\mathcal{G}$, $\mathcal{G}_1$ and $\mathcal{G}_2$, as well as the first and third components of $\mathcal{H}$, $\mathcal{H}_1$ and $\mathcal{H}_3$, are computed as the components of $\mathcal{F}$. The HLL Riemann solver (equation (11)) being a two-wave numerical flux, this assumption is correct only for hyperbolic systems of two equations, such as the one-dimensional shallow water equations. In two space dimensions, there are three equations, hence three eigenvalues (equation (8)). It turns out that in this case the HLL solver described in equation (11) is not precise enough because it involves only two waves. To address this issue, Toro proposed an extension of HLL called the HLLC solver (Toro et al., 1994). The solver we propose in FullSWOF is inspired by this reference, and defines $\mathcal{G}_3$ and $\mathcal{H}_2$ as:

$$\mathcal{G}_3\left(U^n_{i+1/2L,j}, U^n_{i+1/2R,j}\right) =$$

$$\begin{cases} v^n_{i+1/2L,j}\mathcal{G}_1\left(U^n_{i+1/2L,j}, U^n_{i+1/2R,j}\right) & \text{if } u^n_{i+1/2L,j} + u^n_{i+1/2R,j} > 0, \\ v^n_{i+1/2R,j}\mathcal{G}_1\left(U^n_{i+1/2L,j}, U^n_{i+1/2R,j}\right) & \text{if } u^n_{i+1/2L,j} + u^n_{i+1/2R,j} \leq 0, \end{cases}$$

$$\mathcal{H}_2\left(U^n_{i,j+1/2L}, U^n_{i,j+1/2R}\right) =$$

$$\begin{cases} u^n_{i,j+1/2L}\mathcal{H}_1\left(U^n_{i,j+1/2L}, U^n_{i,j+1/2R}\right) & \text{if } v^n_{i,j+1/2L} + v^n_{i,j+1/2R,} > 0, \\ u^n_{i,j+1/2R}\mathcal{H}_1\left(U^n_{i,j+1/2L}, U^n_{i,j+1/2R}\right) & \text{if } v^n_{i,j+1/2L} + v^n_{i,j+1/2R,} \leq 0. \end{cases}$$

4 Description of the FullSWOF Software Package

FullSWOF stands for "Full Shallow Water equations for Overland Flow". The names FullSWOF_1D and FullSWOF_2D define the one-dimensional and the two-dimensional versions, respectively.

FullSWOF having been designed to encourage research reproducibility, the source codes (in C++) are available and can be downloaded from the websites `https://sourcesup.renater.fr/projects/fullswof-1d/` for the one-dimensional version and `https://sourcesup.renater.fr/projects/fullswof-2d/` for the two-dimensional one. The common optional graphic interface is named FullSWOF_UI ("UI" for User Interface), is developed in Java, and is available for download at `https://sourcesup.renater.fr/projects/fullswof-ui/`. Each piece of software is distributed under the CeCILL-V2 (GPL compatible) free software license, which allows to use the software package without any limitation as to its fields of application. For more details, we refer to the documentations on the websites.

The structure of the source code is designed to make future evolutions easy, especially for new developers: for example, a new friction law can easily be added in the libfriction library by creating a new friction file. The documentation for programmers is included directly into the C++ code using doxygen specific comments (van Heesch, 2013). This leads to the automatic extraction of the programmer's manual and simplifies the documenting task. Thanks to the hosting on a software forge, FullSWOF takes benefits of systems of version control, bug tracking, package release, etc.

The one-dimensional program is primarily designed, of course, to carry 1D flow simulations. It is also used as a development tool to test new numerical methods (e.g., fluxes) and to introduce new features in the models (such as new friction and infiltration laws). The new code can then be later integrated into the two-dimensional program: as the 2D mesh is a structured mesh, it is easy to adapt the code from 1D to 2D. Also, a parallel version (MPI) of FullSWOF_2D has been developed in order to run large test cases (such as the Malpasset dam break (section 5)). Currently considered in an early stage of development, it is, at the moment, available only in a dedicated branch of the version control system.

The FullSWOF pieces of software are designed to use point-wise defined topographies and/or initial conditions. At the moment, several topographies and initialization values are hard-coded (e.g., a parabolic topography, the wet dam-break initial data). For other cases, input text files can be read. Friction can be chosen between Manning and Darcy-Weisbach laws. Several boundary conditions are available (e.g., wall, Neumann, periodic, imposed height). The rain is constant in space, but can vary in time. Several numerical methods are implemented for the flux, the linear reconstruction and the order of the scheme. Based on a study of numerical methods for overland flows (Delestre,

2010), default values have been selected for a HLL-type method for the flux, the MUSCL formula for the reconstruction and a second order scheme. We refer to the documentations for more details.

Some classical benchmarks and analytic solutions from the literature are defined in FullSWOF. They have been chosen among the ones gathered in Delestre et al. (2013). They are used to validate each new version of the code before its release, assuring the software quality. This validation is partially automatic thanks to a dedicated script and is useful to both users (who can check their results do not differ from reference results — and do not depend on their compiler, operating system or hardware) and developers (who can check their changes do not cause a regression in the result quality). Additional test cases could be added to validate new conditions introduced in the code.

5 Numerical Illustrations

In this section, we illustrate some results of FullSWOF on a few classical test cases, on analytic solutions available in the literature, and also on three real datasets. This is by no means an analysis of the performances of FullSWOF. It merely aims at demonstrating the ability of FullSWOF to simulate a wide range of flow conditions. In particular, the real datasets in section 5.3 are used without any filtering of the data (no smoothing, etc.). Note that the illustrated test cases and analytic solutions are part of the benchmark set delivered with the FullSWOF_1D or FullSWOF_2D codes. In the following, FullSWOF_1D version 1.01.00 (2013-05-17) and FullSWOF_2D version 1.04.08 (2013-11-07) have been used.

5.1 Classical Test Cases

We begin by running FullSWOF on three analytic cases: one steady state, and two classical transitory solutions. These examples correspond to the original shallow water system with variations in space of the topography: there is no friction, no rain and no infiltration.

5.1.1 Lake at Rest with an Emerged Bump

This one-dimensional steady-state solution has been developed in Delestre (2010) and Delestre et al. (2013, §3.1.2) as a test case for the preservation of steady states and the boundary conditions treatment. It is based on the topography provided by Goutal and Maurel (1997). The initial condition satisfies the hydrostatic equilibrium

$$h + z = \text{const and } q = 0 \text{ m}^2 \text{ s}^{-1}. \tag{14}$$

The domain length is set to $L = 25$ m with a topography given by

$$z(x) = \begin{cases} 0.2 - 0.05(x-10)^2 & \text{if } 8 \text{ m} < x < 12 \text{ m}, \\ 0 & \text{else.} \end{cases}$$

The maximum water height is smaller than the amplitude of the topography in order to simulate a lake at rest with an emerged bump (Figure 4a). In

such a configuration, starting from the steady state, the velocity must remain null and the water surface should stay flat. This is the exact behavior simulated by FullSWOF_1D, showing the interest of a well-balanced scheme (Figure 4).

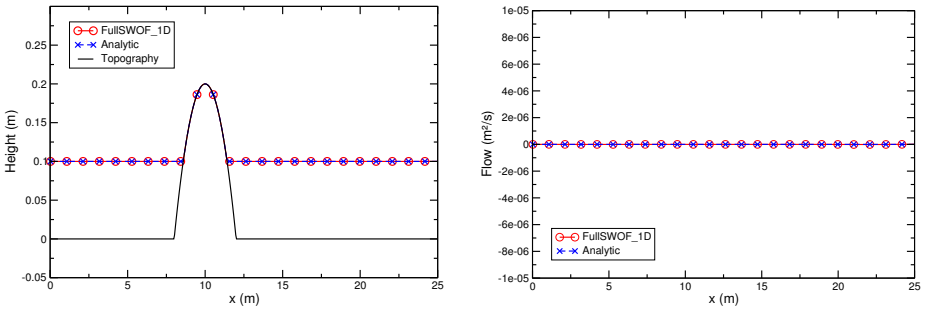

(a) Water heights and topography.

(b) Water fluxes.

Figure 4: Lake at rest with an emerged bump: comparison of the analytic solution with the FullSWOF_1D results. Simulation with 500 cells at T = 100 s.

5.1.2 Dam Break on a Dry Domain without Friction

We turn now to a transitory one-dimensional case, namely the analytic solution of a dam break on a dry domain without friction on a flat and horizontal topography (Delestre et al., 2013, §4.1.2). This case is known as Ritter's solution (Ritter, 1892; Hervouet, 2007). The difficulties here are (a) the existence of a shock, and (b) a wet-dry transition. This case also tests whether the scheme preserves the positivity of the water height, as this property is usually violated near the wetting front.

The initial condition for this configuration is the following Riemann problem

$$h(x) = \begin{cases} h_l = 0.005 \text{ m} & \text{for} \quad 0 \text{ m} \leq x \leq 5 \text{ m}, \\ h_r = 0 \text{ m} & \text{for} \quad 5 \text{ m} < x \leq 10 \text{ m}, \end{cases}$$

with $u(x) = 0 \text{ m s}^{-1}$.

At the beginning of the evolution, the free surface exhibits the following structure: starting from upstream, there is a constant water height at rest (with $h = 0.005$ m) connected by a parabola to a dry zone downstream (with $h = 0$ m). The left extremity of the parabola moves upstream, while its right end slides downstream. Figure 5 displays this solution at time $t = 6$ s.

There is an overall agreement between FullSWOF_1D results and the analytic solution: the code is able to represent the shock, to locate and to treat correctly the wet-dry transition, and to preserve the positivity of the water height. However, differences are observed at the two connections between the constant states and the parabola. These differences get smaller when the space step is decreased (results not shown).

5.1.3 Planar Surface Rotating in a Paraboloid

Finally we present a transitory two-dimensional solution: a planar water surface rotating in a paraboloid (Delestre et al., 2013, §4.2.2). In the literature,

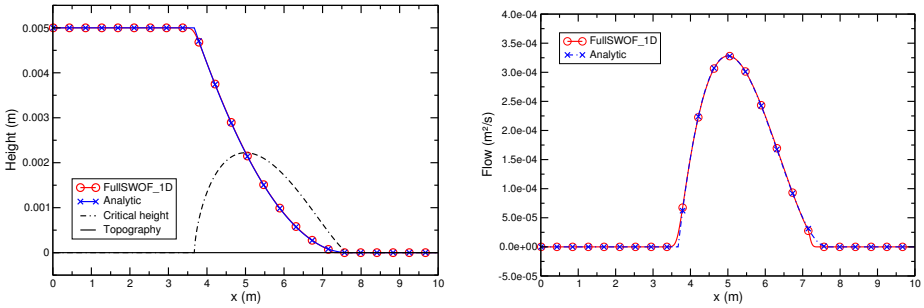

(a) Water heights and topography.

(b) Water fluxes.

Figure 5: Dam break on a dry domain without friction: comparison of the analytic solution with the FullSWOF_1D results. Simulation with 500 cells at T = 6 s.

this analytic solution is known as Thacker's 2D case, named after its author (Thacker, 1981). The topography is a paraboloid of revolution and the shoreline is a moving circle. The free surface has a periodic motion and remains planar in time. To visualize this case, one can think of a glass with some wine in rotation inside (cross-section on Figure 6a). This is a solution with a variable slope (in space) for which the wet-dry transitions are constantly moving. Because there is no friction, the rotation should not damp with time. Hence, this case tests both the ability of the schemes to simulate flow with comings and goings and the numerical diffusion of the scheme (which causes a damping in the water height over time). The analytic solution at $t = 0$ s is taken as initial condition for the computation. The results are considered after three periods.

Overall, FullSWOF_2D gives results in good agreement with the analytic solution (Figure 6). There is no spurious point at the wet-dry transitions, exemplifying the capability of well-balanced schemes to compute properly these common situations for natural surface flows. The slope of the water surface given by FullSWOF_2D is slightly lower than the one of the analytic solution. Also, the water flow is slightly lower than expected. This is a consequence of the numerical diffusion of the scheme. Several techniques could be applied to improve the results of this specific case, but they may not be relevant for the general case, as they would increase the complexity of the method and the computational cost.

5.2 MacDonald Type Solutions

We turn now to a class of stationary solutions, more complex than the previous ones (section 5.1) in the sense that the model is now complete, with friction and rain. These solutions are obtained by the procedure introduced by I. MacDonald: the water height profile and the discharge are given and the corresponding topography is then computed. In the original works, the Manning friction law was considered (MacDonald, 1996; MacDonald et al., 1997), but the method allows many variants: other friction laws, rain, diffusion, etc.

The three selected solutions show the ability of a scheme to cope with stationary states induced by topography and friction in a wide range of flow con-

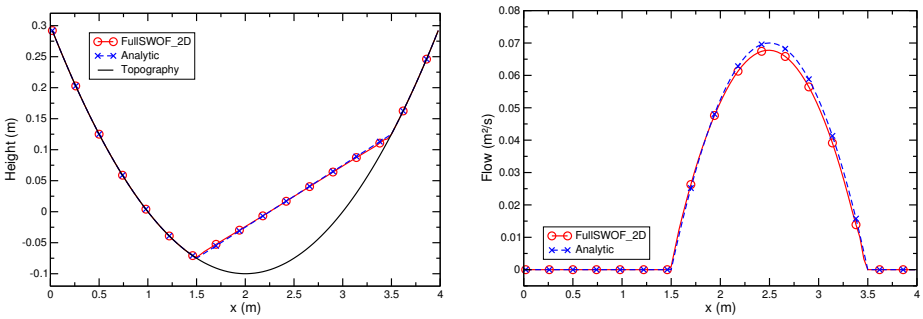

(a) Water heights and topography.

(b) Water fluxes.

Figure 6: Planar surface rotating in a paraboloid: comparison of the analytic solution with the FullSWOF_2D results. Cross-sections at $y = 2$ m. Simulation with 100 cells in x and y, at T = 13.4571 s.

ditions.

5.2.1 Short Channel with a Smooth Transition and a Shock

The length of the channel is 100 m and the discharge at steady state is $q = 2\ \mathrm{m^2\,s^{-1}}$ (Figure 7). The flow is subcritical both upstream and downstream (Delestre et al., 2013, §3.2.2). In the intermediate part, the flow is supercritical. Hence, the flow goes from subcritical to supercritical via a sonic point, and then — through a shock (located at $x = 200/3 \approx 66.67$ m) — becomes subcritical again (Figure 7a). The Manning friction coefficient n is equal to 0.0328 $\mathrm{m^{-1/3}\,s}$. The run was carried out with a resolution of 0.2 m.

The water flow simulated by FullSWOF_1D matches the analytic solution except at the shock (Figure 7b). A careful examination showed the mismatch is limited to two cells. This is a numerical artifact due to the product of approximations of two discontinuous functions (u and h) on a discretization grid. Further testing showed the shock was better represented with finer grids, which is the expected behavior. Future developments — by us or by others, since FullSWOF is a free software — could improve the result of this test case.

5.2.2 Rain on a Long Channel with a Supercritical Flow

This analytic case is similar to the previous one, but includes rain (Delestre et al., 2013, §3.3.2). The channel length is set equal to 1000 m (Figure 8). As the flow is supercritical along the whole channel, we consider a constant discharge and a constant water height at inflow and a free outflow. In the simulation, at initial time, the channel is dry. There is no rain until 1500 s; after this moment, the rain intensity is set to 0.001 $\mathrm{m\,s^{-1}}$ until the end. The Darcy-Weisbach friction coefficient is $f = 0.065$ and the inflow discharge is $q_0 = 2.5\ \mathrm{m^2\,s^{-1}}$ (Figure 8).

FullSWOF_1D results match quite well the analytic solution, showing the inclusion of the rain source term in the model and its implementation in the code are satisfactory.

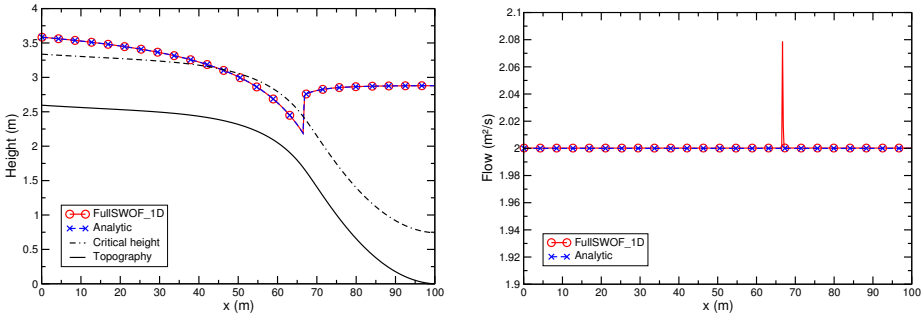

(a) Water depths and topography. (b) Water fluxes.

Figure 7: Short channel with a smooth transition and a shock: comparison of the analytic solution with the FullSWOF_1D results. Simulation with 500 cells at T = 1500 s.

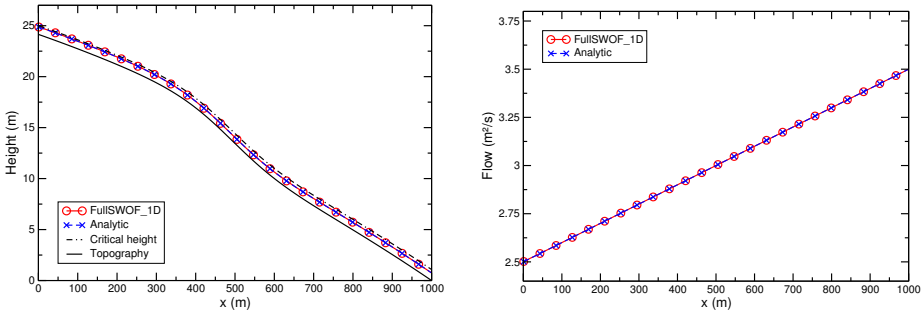

(a) Water heights and topography. (b) Water fluxes.

Figure 8: Rain on a long channel with a supercritical flow: comparison of the analytic solution with the FullSWOF_1D results. Simulation with 500 cells in x at T = 3000 s.

5.2.3 Pseudo-2D Channel with a Supercritical Flow

In this section, we consider a pseudo-2D shallow water system in a channel with a varying width. By pseudo-2D we mean an intermediate model between the one-dimensional and the two-dimensional models. More precisely, the pseudo-2D shallow water equations are obtained by averaging all quantities both in the vertical direction and on the width of the channel ($y-$direction), i.e., on the perpendicular to the flow (recall that the two-dimensional shallow water equations involve an average solely in the vertical direction). The derivation is detailed in Goutal and Sainte-Marie (2011). In this paper, the authors showed that the new terms that appear in the pseudo-2D shallow water system due to the y-averaging bring numerical difficulties that must be treated carefully. We perform a simulation of the full two-dimensional equations with a topography and a discharge corresponding to a stationary state for the pseudo-2D system, which allows some comparisons.

We consider a 200-m long channel with a rectangular cross-section. The width and the slope of the channel depend on x (Figure 9a). The flow is fixed at inflow $q = 20$ m^3 s^{-1} and the water height is prescribed at outflow (Delestre et al., 2013, §3.5.2). The Manning coefficient is set to 0.03 m$^{-1/3}$ s. The channel is initially dry, with a little puddle downstream (because of the outflow condition).

At steady state, FullSWOF_2D produces a depth profile similar to the analytic solution (Figure 9b). In fact, an exact match is not to be expected since the results of a 2D code are compared with the analytic solution of a *pseudo*-2D case.

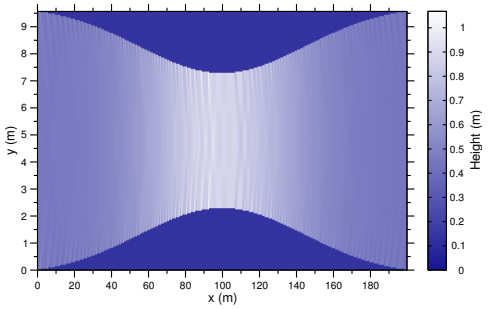

(a) Water height simulated by FullSWOF_2D. Inside the channel, the water height ranges from 0.38 m to 1.07 m.

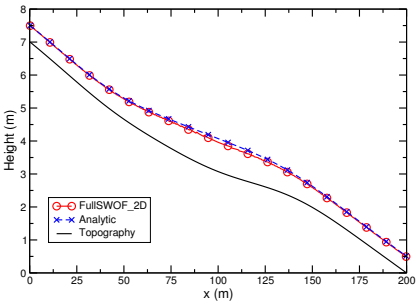

(b) Water heights. For FullSWOF_2D, the mean height inside the channel is plotted.

Figure 9: Pseudo-2D channel with a supercritical flow: comparison of the analytic solution with the FullSWOF_2D results. Simulation with 400 cells in x and 201 cells in y, at T = 200 s.

5.3 Real Datasets

Finally, we give the results of FullSWOF on three real datasets. The first case is an original laboratory experiment, the second one comes from an experimental plot in Senegal, and the third is the well-known Malpasset dam break. We do not pretend to give new insights about the occurring phenomena, but merely

show the ability of FullSWOF to simulate real situations without data filtering. Refined calibration of the parameters and comparison with other piece of softwares will be the topic of future works.

5.3.1 Flow over a Corrugated Bottom

This first example is an experimental flow over an inclined channel having a corrugated bottom (Figure 10). The discharge is imposed upstream (measured value: $0.69\,\mathrm{l\,m^{-1}\,s^{-1}}$). Water heights are measured at steady state along a 55-cm long profile with a 0.5-mm resolution using the device described in Legout et al. (2012). FullSWOF_1D is run using the measured topography profile as input. The only calibrated parameter is the Manning friction coefficient $n = 0.0127\ \mathrm{m^{-1/3}\,s}$.

The comparison of the computed and measured values shows that FullSWOF_1D is able to reproduce the qualitative behavior after the first bump ($x > 0.06$ m) (Figure 10b). FullSWOF_1D reproduces all the hydraulic jumps (for $x > 0.13$ m) and locates them correctly at the minima of the measured solution. However, the simulated solution exhibits shocks which are steeper than the measured ones. This, as well as the poor restitution at the beginning of the channel (around $x = 0.05$ m), is probably due to a lack in the model. Indeed, in this range of water heights and velocities, the surface tension likely cannot be neglected. This is a possible extension of the FullSWOF software.

(a) Close-up photography of the experimental setup. The red line is the measured profile.

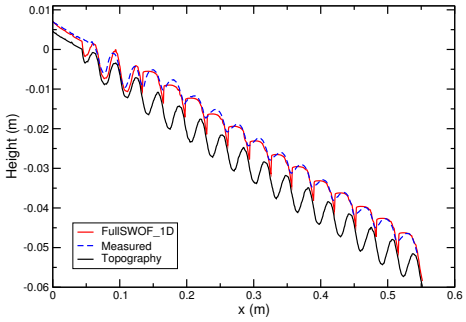

(b) Measured topography, experimental water surface and water surface computed by FullSWOF_1D (Simulation with 1104 cells at T = 10 s).

Figure 10: Experimental flow over a corrugated bottom.

5.3.2 Rain over a Field Plot (Thiès, Senegal)

The purpose of this section is to confront FullSWOF_2D to a real system: the plot of Thiès, Senegal (Tatard et al., 2008; Mügler et al., 2011), an experimental system instrumented by IRD. It consisted in an artificial rainfall of about 2 hours with an intensity close to 70 $\mathrm{mm\,h^{-1}}$ on a sandy-soil plot of 4×10 $\mathrm{m^2}$. The plot had the classical configuration of Wooding's open book, with 1% slope along Ox and Oy axes. The complete dataset is freely available at `http://www.umr-lisah.fr/Thies_2004/`. FullSWOF_2D is used with a variable time step

(the CFL value is fixed at 0.4) and with the same parameters as in Tatard et al. (2008): $f = 0.26$, $h_f = 0.06$ m, $\theta_s - \theta_i = 0.12$, $K_s = 4.4\ 10^{-6}$ m s^{-1} and $K_c = 0$.

Qualitatively, the results (Figure 11) are similar to the ones obtained with other pieces of software (Tatard et al., 2008; Mügler et al., 2011). At this stage, these results illustrate the ability of FullSWOF_2D to simulate a dynamic flow without any filtering of the data, contrarily with the previously-used pieces of software. A comparison will be carried out in a more detailed study.

5.3.3 The Malpasset Dam Break: a Large Dataset Demanding the Parallel Version of FullSWOF_2D

This section is devoted to a large scale test case. This is the well-known Malpasset dam break, that actually happened in 1959 in the south of France (Hervouet (2000), Hervouet (2007, p.281-288)). Because of its varying topography and complex geometry, this is a classical test for numerical methods and hydraulics software validation. For this case, we used the parallel version of FullSWOF_2D (Cordier et al., shed), in order to have only a few hours of computation. The dimensions of the computing domain are $L_x = 17273.9$ m with 1000 cells and $L_y = 8381.3$ m with 486 cells. The topography comes from a map published before the disaster and then digitized. We consider the Manning law with $n = 0.033$ m$^{-1/3}$ s as advised in Hervouet (2000). No calibration was done for this simulation, which has a total time of T = 4000 s.

The results are presented in Figure 12 a–d at four time steps. A scaled physical experiment was built by the Laboratoire National d'Hydraulique in 1964, in order to study the dam-break flow (for more details see Hervouet (2000) and Hervouet (2007)). The maximum water level was recorded at nine gauges (named from 6 to 14) during the physical experiment (Figure 12e). The maximum water elevations of the scaled experiment are quite well captured by FullSWOF_2D (Figure 12f).

6 Conclusions

The FullSWOF software project grew out of a long-time collaboration between mathematicians and hydrologists in Orléans (France). Several specific features make it particularly suitable for applications in hydrology: it takes into account rain, infiltration, classical frictions laws, and can operate with DEMs. Moreover it has shown its ability to deal with a wide range of flow conditions. The last releases of its three codes (FullSWOF_1D, FullSWOF_2D and FullSWOF_UI) are fairly stable and robust. They are freely available for people outside the original team for industrial, scientific and educational purposes.

The project is still undergoing several improvements. Apart from the usual bug correction work, several ameliorations on the current codes (e.g., non-homogeneous friction) are regularly performed and a parallel 2D version is under development. More conceptual modifications are under consideration, such as the introduction of erosion and sedimentation models. Another direction of improvement concerns the surface tension. While, at the moment, these modifications originate mainly from the initial development team, we emphasize that external contributions are welcome.

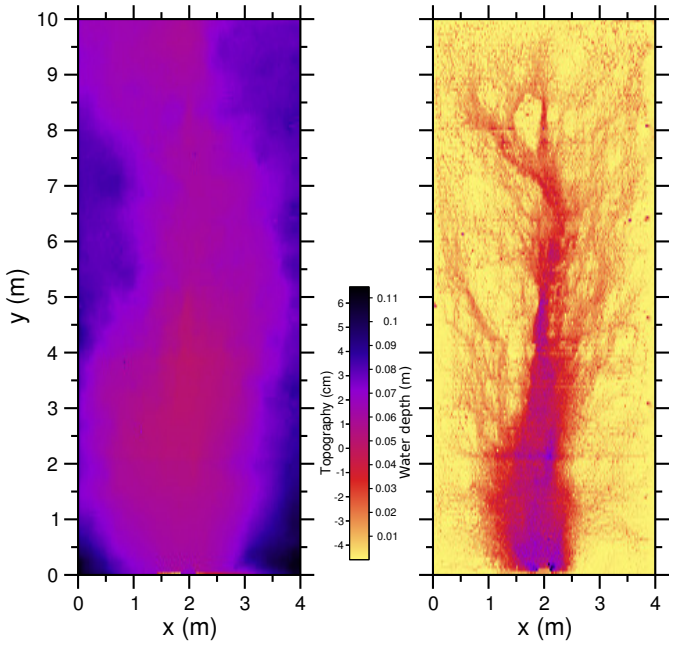

(a) Topography (without the 1% slope along y).

(b) Water depth.

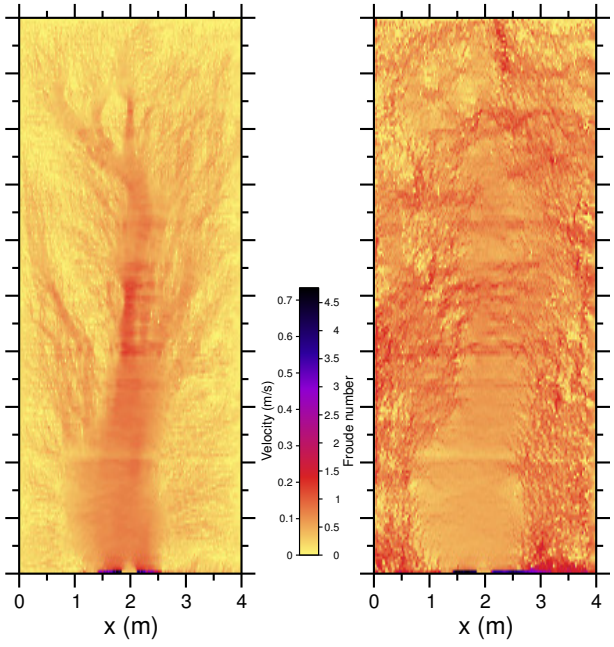

(c) Velocity.

(d) Froude number.

Figure 11: Results of FullSWOF_2D for the Thiès field plot. Simulation with 160 cells in x and 200 cells in y, at T = 7400 s.

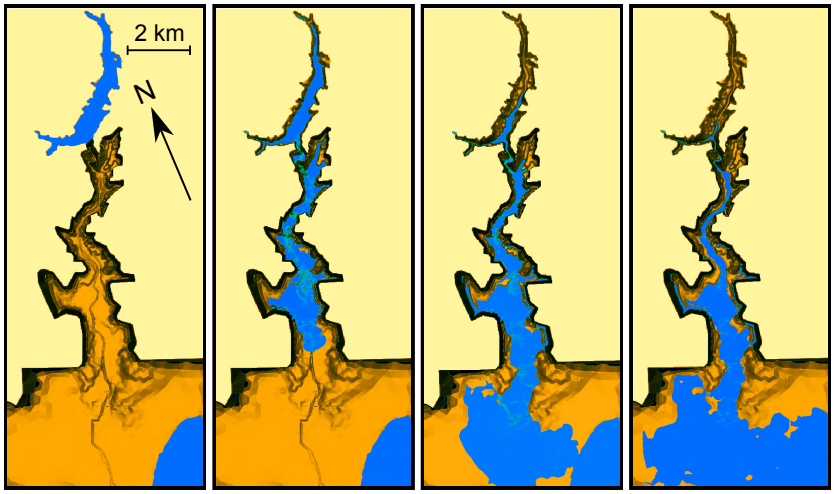

(a) t = 0 s (b) t =1000 s. (c) t =2500 s. (d) t = 4000 s.

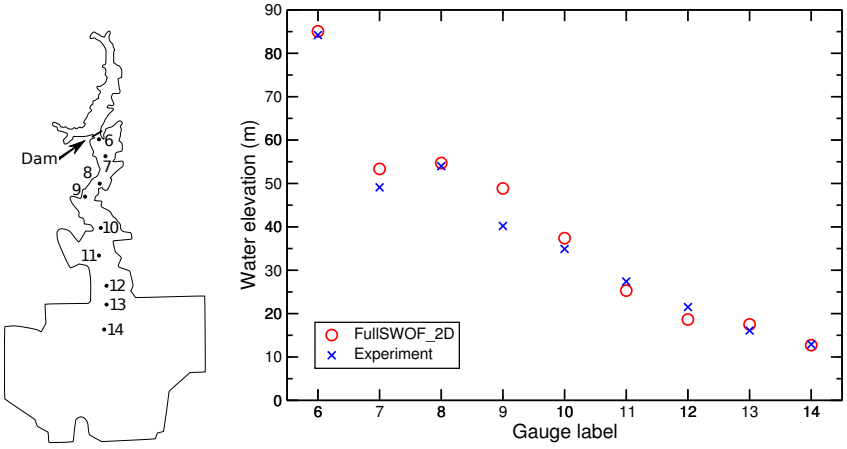

(e) Gauge location. (f) Comparison of maximal water elevations

Figure 12: Malpasset dam break: evolution of the water flow simulated by FullSWOF_2D (parallel version), and comparison with experimental data.

7 Acknowledgments

This study is part of the ANR METHODE granted by the French National Agency for Research, ANR-07-BLAN-0232. The authors would like to thank Olivier Planchon (IRD) for the data used in Section 5.3.2.

References

Audusse, E., Bouchut, F., Bristeau, M.-O., Klein, R., and Perthame, B. (2004). A fast and stable well-balanced scheme with hydrostatic reconstruction for shallow water flows. *SIAM J. Sci. Comput.*, 25(6):2050–2065.

Baartman, J. E. M., Temme, A. J. A. M., Veldkamp, T., Jetten, V. G., and Schoorl, J. M. (2013). Exploring the role of rainfall variability and extreme events in long-term landscape development. *Catena*, 109:25–38.

Barnes, N. (2010). Publish your computer code: it is good enough. *Nature*, 467(7317):753.

Barré de Saint-Venant, A.-J.-C. (1871). Théorie du mouvement non-permanent des eaux, avec application aux crues des rivières et à l'introduction des marées dans leur lit. *Comptes Rendus de l'Académie des Sciences*, 73:147–154.

Batten, P., Clarke, N., Lambert, C., and Causon, D. M. (1997). On the choice of wavespeeds for the HLLC Riemann solver. *SIAM J. Sci. Comput.*, 18(6):1553–1570.

Berger, M. J., George, D. L., LeVeque, R. J., and Mandli, K. T. (2011). The GeoClaw software for depth-averaged flows with adaptive refinement. *Advances in Water Resources*, 34:1195–1206.

Bermúdez, A. and Vázquez, M. E. (1994). Upwind methods for hyperbolic conservation laws with source terms. *Computers & Fluids*, 23(8):1049–1071.

Bouchut, F. (2004). *Nonlinear Stability of Finite Volume Methods for Hyperbolic Conservation Laws, and Well-Balanced Schemes for Sources*. Frontiers in Mathematics. Birkhäuser Basel.

Bristeau, M.-O. and Coussin, B. (2001). Boundary conditions for the shallow water equations solved by kinetic schemes. Technical Report RR-4282, INRIA.

Brunner, G. W. (2010). *HEC-RAS River Analysis System. Hydraulic Reference Manual Version 4.1*. US Army Corps of Engineers. Hydrologic Engineering Center, Davis, CA, USA, cpd-69 edition.

Chow, V. T. (1959). *Open-Channel Hydraulics*. McGraw-Hill, New York.

Claerbout, J. and Karrenbach, M. (1992). Electronic documents give reproducible research a new meaning. In *Proceedings of the 62nd Annual International Meeting of the Society of Exploration Geophysics*, pages 601–604.

Cordier, S., Coullon, H., Delestre, O., Laguerre, C., Le, M. H., Pierre, D., and Sadaka, G. (To be published). FullSWOF_paral: comparison of two parallelization strategies (MPI and SkelGIS) on a software designed for hydrology applications. In *ESAIM: Proc. CEMRACS'12: Numerical Methods and Algorithms for High Performance Computing*.

Delestre, O. (2010). *Rain water overland flow on agricultural fields simulation*. PhD thesis, University of Orléans, France. In French.

Delestre, O., Cordier, S., Darboux, F., and James, F. (2012). A limitation of the hydrostatic reconstruction technique for Shallow Water equations. *Comptes Rendus de l'Académie des Sciences - Série I - Mathématique*, 350:677–681.

Delestre, O., Cordier, S., James, F., and Darboux, F. (2009). Simulation of rainwater overland-flow. In Tadmor, E., Liu, J.-G., and Tzavaras, A., editors, *Proceedings of the* 12^{th} *International Conference on Hyperbolic Problems*, volume 67 of *Proceedings of Symposia in Applied Mathematics*, pages 537–546, University of Maryland, College Park (USA). Amer. Math. Soc.

Delestre, O. and James, F. (2010). Simulation of rainfall events and overland flow. In *Proceedings of* 10^{th} *International Conference Zaragoza-Pau on Applied Mathematics and Statistics, Jaca, Spain*, volume 35 of *Monografías Matemáticas García de Galdeano*, pages 125–135.

Delestre, O., Lucas, C., Ksinant, P.-A., Darboux, F., Laguerre, C., Vo, T. N. T., James, F., and Cordier, S. (2013). SWASHES: a compilation of Shallow-Water analytic solutions for hydraulic and environmental studies. *International Journal for Numerical Methods in Fluids*, 72:269–300.

DHI Software (2009). *MIKE 11. A Modelling System for Rivers and Channels. Reference Manual*. Denmark.

Esteves, M., Faucher, X., Galle, S., and Vauclin, M. (2000). Overland flow and infiltration modelling for small plots during unsteady rain: numerical results versus observed values. *Journal of Hydrology*, 228(3–4):265–282.

Fiedler, F. R. and Ramirez, J. A. (2000). A numerical method for simulating discontinuous shallow flow over an infiltrating surface. *International Journal for Numerical Methods in Fluids*, 32(2):219–239.

Godlewski, E. and Raviart, P.-A. (1996). *Numerical approximation of hyperbolic systems of conservation laws*, volume 118 of *Applied Mathematical Sciences*. Springer-Verlag, New York, USA.

Goutal, N. and Maurel, F. (1997). Proceedings of the 2^{nd} workshop on dambreak wave simulation. Technical Report HE-43/97/016/B, Electricité de France, Direction des études et recherches.

Goutal, N. and Sainte-Marie, J. (2011). A kinetic interpretation of the section-averaged Saint-Venant system for natural river hydraulics. *International Journal for Numerical Methods in Fluids*, 67(7):914–938.

Green, W. H. and Ampt, G. A. (1911). Studies on soil physics. part I.—the flow of air and water through soils. *The Journal of Agricultural Science*, 4(1):1–24.

Greenberg, J. M. and LeRoux, A. Y. (1996). A well-balanced scheme for the numerical processing of source terms in hyperbolic equation. *SIAM Journal on Numerical Analysis*, 33:1–16.

Halcrow (2012). *ISIS 2D quick start guide — v. 3.6*.

Harten, A., Lax, P. D., and van Leer, B. (1983). On upstream differencing and Godunov-type schemes for hyperbolic conservation laws. *SIAM Review*, 25(1):35–61.

Hervouet, J.-M. (2000). A high resolution 2-D dam-break model using parallelization. *Hydrological Processes*, 14(13):2211–2230.

Hervouet, J.-M. (2007). *Hydrodynamics of free surface flows*. Wiley.

Hillel, D. and Gardner, W. R. (1970). Transient infiltration into crust-topped profiles. *Soil Science*, 109(2):69–76.

Lee, S.-H. and Wright, N. G. (2010). Simple and efficient solution of the shallow water equations with source terms. *International Journal for Numerical Methods in Fluids*, 63:313–340.

Legout, C., Darboux, F., Nédélec, Y., Hauet, A., Esteves, M., Renaux, B., Denis, H., and Cordier, S. (2012). High spatial resolution mapping of surface velocities and depths for shallow overland flow. *Earth Surface Processes and Landforms*, 37(9):984–993.

Liang, Q. and Marche, F. (2009). Numerical resolution of well-balanced shallow water equations with complex source terms. *Advances in Water Resources*, 32(6):873–884.

MacDonald, I. (1996). *Analysis and computation of steady open channel flow*. PhD thesis, University of Reading — Department of Mathematics.

MacDonald, I., Baines, M. J., Nichols, N. K., and Samuels, P. G. (1997). Analytic benchmark solutions for open-channel flows. *Journal of Hydraulic Engineering*, 123(11):1041–1045.

Mangeney, A., Bouchut, F., Thomas, N., Vilotte, J.-P., and Bristeau, M.-O. (2007). Numerical modeling of self-channeling granular flows and of their levee-channel deposits. *Journal of Geophysical Research*, 112(F2):F02017.

Mein, R. G. and Larson, C. L. (1973). Modeling infiltration during a steady rain. *Water Resources Research*, 9(2):384–394.

Moussa, R. and Bocquillon, C. (2000). Approximation zones of the Saint-Venant equations for flood routing with overbank flow. *Hydrology and Earth System Sciences*, 4(2):251–260.

Mügler, C., Planchon, O., Patin, J., Weill, S., Silvera, N., Richard, P., and Mouche, E. (2011). Comparison of roughness models to simulate overland flow and tracer transport experiments under simulated rainfall at plot scale. *Journal of Hydrology*, 402(1–2):25–40.

Novak, P., Guinot, V., Jeffrey, A., and Reeve, D. E. (2010). *Hydraulic modelling — An Introduction. Principles, Methods and Applications*. Spon Press.

Paquier, A. (1995). *Modeling and simulation of the propagation of the dam-break wave*. PhD thesis, University of Saint-Etienne, France. In French.

Peng, R. D. (2011). Reproducible research in computational science. *Science*, 334(6060):1226–1227.

Popinet, S. (2011). Quadtree-adaptative tsunami modelling. *Ocean Dynamics*, 61(9):1261–1285.

Ritter, A. (1892). Die Fortpflanzung der Wasserwellen. *Zeitschrift des Vereines Deuscher Ingenieure*, 36(33):947–954.

Stodden, V., Bailey, D. H., Borwein, J., LeVeque, R. J., Rider, W., and Stein, W. (2013). Setting the default to reproducible: Reproducibility in computational and experimental mathematics. Technical report, Institute for Computational and Experimental Research in Mathematics.

Tanguy, J.-M. and Chocat, B. (2013). *CANOE*, pages 209–218. John Wiley & Sons, Inc.

Tatard, L., Planchon, O., Wainwright, J., Nord, G., Favis-Mortlock, D., Silvera, N., Ribolzi, O., Esteves, M., and Huang, C. (2008). Measurement and modelling of high-resolution flow-velocity data under simulated rainfall on a low-slope sandy soil. *Journal of Hydrology*, 348(1-2):1–12.

Thacker, W. C. (1981). Some exact solutions to the nonlinear shallow-water wave equations. *Journal of Fluid Mechanics*, 107:499–508.

Toro, E., Spruce, M., and Speares, W. (1994). Restoration of the contact surface in the HLL-Riemann solver. *Shock Waves*, 4:25–34.

van Heesch, D. (2013). *doxygen. Manual for version 1.8.5*.

Zhang, W. and Cundy, T. W. (1989). Modeling of two-dimensional overland flow. *Water Resources Research*, 25(9):2019–2035.